The suitability of hybrid meshes for low-Mach large-eddy simulation

By S. P. Domino†, L. Jofre AND G. Iaccarino

A computational simulation study for a turbulent plane channel, $Re_\tau = 180$, is presented to evaluate the suitability of hybrid meshes for low-Mach large-eddy simulation. A structured/orthogonal homogeneous mesh composed of hexahedral elements is compared with a heterogeneous, unstructured hybrid mesh that includes hexahedral, tetrahedral, pyramid, and wedge element topologies. The low-Mach, low-dissipation methodology compares edge- and element-based vertex-centered finite-volume discretization methods. Simulations with and without a subgrid-scale large-eddy simulation model are conducted in the context of a solution verification methodology. Results indicate that on ideal hexahedral meshes, the element-based scheme predicts (on average) better mean streamwise velocity and root mean square (rms) velocity profiles, but at an increased computational cost of approximately twofold. For the generalized unstructured hybrid mesh, low-order statistics are predicted to be symmetric for both schemes; however, asymmetry for higher-order statistics is observed. In general, the asymmetric nature of the edge-based scheme is more pronounced than for the element-based scheme, while overall predictions appear to have lower dissipation when using the element-based approach, which is accompanied by a similar (i.e., approximately twofold) increase in computational cost.

1. Introduction

Facilitated by the development of massively parallel computing architectures, low-Mach large-eddy simulation (LES) studies continue to be deployed as a production tool to support a variety of complex applications ranging from multi-physics fire applications (Hanlin *et al.* 2009) to wind energy (Domino 2018). However, many industrial applications of interest require the resolution of complex geometrical features that, in practice, drives usage of so-called hybrid meshes. A hybrid mesh is simply defined as a heterogeneous mesh composed of combinations of hexahedral, tetrahedral, pyramid, and wedge elements. Several unstructured methodologies have been deployed in the open literature and are routinely used for geometrically complex use cases that employ finite-element (Jansen 1996), vertex-centered finite-volume (Domino 2018), or cell-centered approaches (Mahesh *et al.* 2004).

Given the extensive use of generalized unstructured methods, the open literature includes a limited number of low-Mach detailed validation comparisons between ideal hexahedral-based topologies and hybrid mesh strategies (see de Wiart *et al.* 2014 for an example). In 2006, a comparison between a cell-centered and a vertex-centered finite-volume method was conducted for an $Re_\tau = 180$ turbulent plane channel (Ham *et al.* (2006)). Results from this foundational study indicated that on hybrid meshes, the implemented cell-centered approach did not retain symmetry for the mean streamwise velocity profile. By comparison, the vertex-based scheme demonstrated an improved symmetric mean velocity profile.

† Computational Thermal and Fluid Mechanics, Sandia National Laboratories

In this paper, we provide a simulation study for an $Re_\tau = 180$ turbulence channel flow that includes both ideal homogeneous hexahedral-based meshes and the replicated hybrid mesh outlined by Ham *et al.* (2006). Simulations are run using low-order edge- and element-based vertex-centered finite-volume schemes. For the edge-based scheme, care is taken to ensure that the diffusion operator treats non-orthogonality between the edge distance vector and the assembled area vector in a robust manner (see, e.g., Jasak 1996). Although the element-based approach lends itself to higher-order hexahedral approaches, the study described in this paper is limited to low-order element types, i.e., second-order spatial and temporal accuracy.

In Section 2, the governing equations in addition to a high-level discretization overview are provided. Primary simulation study results for the plane channel simulation are given in Section 3. Finally, conclusions are provided in Section 4.

2. Low-Mach equation set

For completeness, we present the generalized low-Mach equation set, noting that for the particular plane channel test case, the density and viscosity are constant. The integral form of the Favre-filtered variable-density continuity to be solved is

$$\int \frac{\partial \bar{\rho}}{\partial t} \mathrm{d}V + \int \bar{\rho} \tilde{u}_j \mathrm{d}S = 0. \tag{2.1}$$

In the above equation, $\bar{\rho}$ is the fluid density and $\tilde{u}_j$ is the density-weighted, i.e., Favre-averaged, fluid velocity.

The momentum equation used for LES turbulent transport, also in integral form, is

$$\int \frac{\partial \bar{\rho} \tilde{u}_i}{\partial t} \mathrm{d}V + \int \bar{\rho} \tilde{u}_i \tilde{u}_j n_j \mathrm{d}S = \int \tilde{\sigma}_{ij} n_j \mathrm{d}S - \int \tau_{ij}^{sgs} n_j \mathrm{d}S, \tag{2.2}$$

where the subgrid-scale (SGS) turbulent stress τ_{ij}^{sgs} is defined as

$$\tau_{ij}^{sgs} \equiv \bar{\rho}(\widetilde{u_i u_j} - \tilde{u}_i \tilde{u}_j). \tag{2.3}$$

The Cauchy stress is provided by

$$\sigma_{ij} = 2\mu \tilde{S}_{ij}^{*} - \bar{P}\delta_{ij}, \tag{2.4}$$

where the traceless rate-of-strain tensor is defined as

$$\tilde{S}_{ij}^{*} = \tilde{S}_{ij} - \frac{1}{3}\delta_{ij}\tilde{S}_{kk} = \tilde{S}_{ij} - \frac{1}{3}\frac{\partial \tilde{u}_k}{\partial x_k}\delta_{ij}.$$

In a low-Mach flow, the above pressure, $\bar{P}$, is the perturbation about the thermodynamic pressure, P^{th}. For LES, τ_{ij}^{sgs} which appears in Eq. (2.2) and is defined in Eq. (2.3) represents the SGS stress tensor that must be closed. The deviatoric part of the subgrid stress tensor is defined as $\tau_{ij}^{*sgs} = \tau_{ij}^{sgs} - 1/3\delta_{ij}\tau_{kk}^{sgs}$, where the SGS turbulent kinetic energy is given by $\tau_{kk}^{sgs} = 2\bar{\rho}k$. Here, k represents the modeled turbulent kinetic energy, formally defined as $\bar{\rho}k = 1/2\bar{\rho}(\widetilde{u_k u_k} - \tilde{u}_k\tilde{u}_k)$. Above, $|\tilde{S}| = \sqrt{2\tilde{S}_{ij}\tilde{S}_{ij}}$. The turbulence case presented in this paper uses the wall-adapting local eddy viscosity (WALE) model (Nicoud & Ducros 1999) for the isotropic eddy-viscosity closure model.

2.1. *Numerical implementation*

The low-Mach method used in this paper can be classified as an equal-order, pressure-stabilized, approximate-pressure projection-based scheme (Domino 2006). Pressure sta-

bilization, due to the equal-order interpolation methodology, is achieved by adding a scaled fine-scale momentum residual to the continuity equation that has been adapted for a vertex-centered finite-volume method. The control-volume finite-element method (CVFEM) is used to define a dual mesh for all of the supported element topologies that include low-order hexahedral, tetrahedral, pyramid, and wedge elements. When the edge-based scheme is used, sub-control surface area vectors and sub-control volumes are assembled to the edges and nodes, respectively. Time advancement is achieved using a three-state, second-order BDF2 time integrator. Due to space limitations, we refer the reader seeking a complete overview of the underlying numerical implementation, including detailed code verification, to previous papers (Domino 2014a; Domino 2018) and the Nalu theory manual, (Domino 2014b).

3. LES channel $Re_\tau = 180$

In this section, simulation results are provided with and without the SGS model for the Hex8 and hybrid mesh topologies for the Re_τ plane channel flow results versus established direct numerical simulation (DNS) results (Moser *et al.* 1999). As is customary, $Re_\tau = u_\tau \delta/\nu$, where u_τ is the friction velocity, δ is the channel half-height, and ν is the kinematic viscosity of the fluid; $\nu = \mu/\rho$, with μ the dynamic viscosity and ρ the density.

The mass flow rate is imposed through a mean streamwise pressure gradient, $\langle \mathrm{d}p/\mathrm{d}x \rangle = -\tau_w/\delta$, where p is the pressure and $\tau_w = \rho\nu \left(\mathrm{d}\langle u \rangle/\mathrm{d}y\right)_{y=0} = \rho u_\tau^2$ is the wall shear stress, with $\langle u \rangle$ the mean streamwise velocity. The computational domain is $4\pi\delta \times 2\delta \times 4/3\pi\delta$ in the streamwise (x), vertical (y), and spanwise (z) directions, respectively. The streamwise and spanwise boundaries are set periodic, and no-slip conditions are imposed on the horizontal boundaries (x–z planes). The grid is uniform in the streamwise and spanwise directions with spacing (in wall units) equal to $\Delta x^+ = 24$ and $\Delta z^+ = 18$, and stretched toward the walls in the vertical direction with the first grid point at $y^+ = y u_\tau/\nu = 0.17$. This grid arrangement corresponds to a mesh of size $96 \times 96 \times 64$ grid points. For the hybrid mesh, which includes Hex8, Tet4, Pyramid5, and Wedge6, near-wall mesh spacing replicates that of the structured Hex8 mesh. However, the domain in the wall-normal direction is cut in half. The bottom section retains the Hex8-based mesh, while the top section uses a Wedge6 near-wall mesh that transitions to a Tet4 block. The conformal interface between the Tet4 and Hex8 blocks is retained through the use of the Pyramid5 transition element. Figure 1 provides a plot of the normalized LES filter length, Δ^+, as a function of normalized distance, y^+, from the lower wall (for the hybrid mesh) and also includes a view of the active mesh lines for both the structured Hex8 and the hybrid meshes. In this figure, normalization is based on the channel half-width. For the hybrid mesh section, the dual LES filter within the Tet4 mesh region is approximately 1.5 times larger than the baseline Hex8 and Wedge6 homogeneous blocks. Note that the transitioned filter for the hybrid mesh is abrupt and highly non-symmetric.

The simulation strategy starts from a sinusoidal velocity field which is advanced in time to reach turbulent steady-state conditions after several flow-through times (FFTs); on the basis of the bulk velocity, $u_b = 1/\delta \int_0^\delta \langle u \rangle \, \mathrm{d}y$, and the length of the channel, $L = 4\pi\delta$, an FTT is defined as $t_b = L/u_b$. Once a sufficiently long transient period has surpassed — approximately 10 eddy-turnover times, $t_l \sim \delta/u_\tau$ —, first- and second-order statistics are collected. Advection stabilization is not used in these simulations.

The accuracy of the methods is analyzed by calculating time- and space-averaged (x and z directions) first- and second-order flow statistics. The quantities of interest (QoIs)

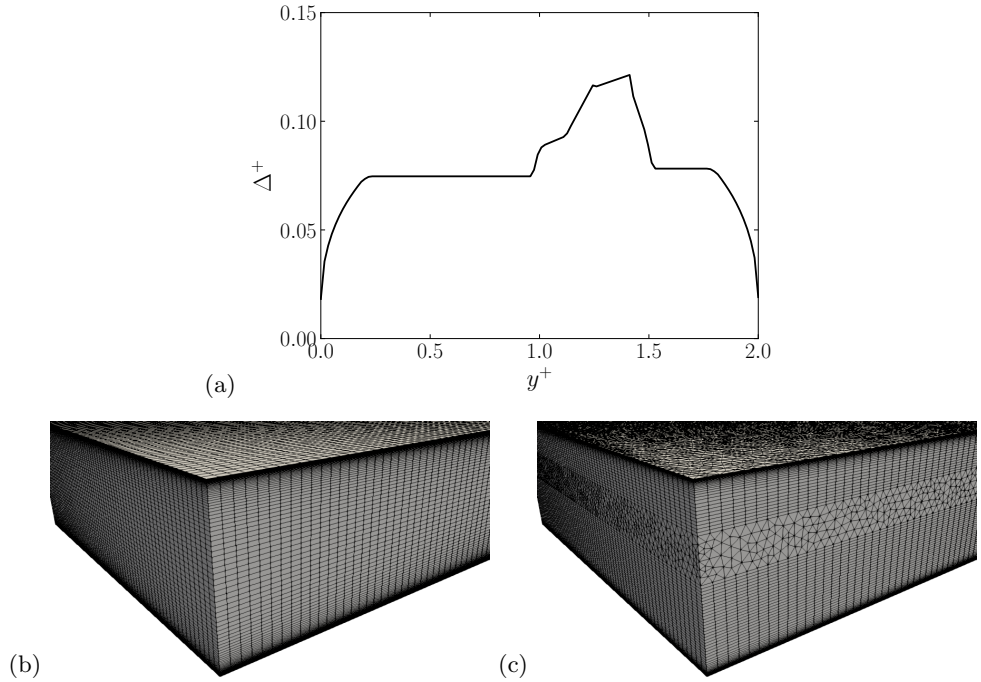

FIGURE 1. Base refinement mesh for the structured Hex8 and hybrid meshes. LES filter size (a), and structured Hex8 (b) and unstructured hybrid (c) meshes.

considered are the numerical friction, Re_τ, and bulk, $Re_b = 2u_b\delta/\nu$, Reynolds numbers; the skin-friction coefficient, $C_f = \tau_w/(1/2\rho u_b^2)$; the mean streamwise velocity profile, $u^+ = \langle u \rangle / u_\tau$; and the root mean square (rms) velocity fluctuations, u^+_{rms}, v^+_{rms}, and w^+_{rms}. Reference solutions for all these QoIs are available in the literature. For instance, Re_b can be analytically approximated from $Re_\tau \approx 0.09 Re_b^{0.88}$ (Pope 2000). Once Re_b is known, C_f is directly obtained by calculating u_b from the bulk Reynolds number definition and noticing that τ_w and ρ depend on $\langle \mathrm{d}p/\mathrm{d}x \rangle$ and Re_τ. For the structured Hex8, postprocessing is achieved through the direct query of degree-of-freedom nodal locations while for the hybrid mesh, interpolation of the mean flow field to a series of planes parallel to the no-slip wall boundaries is used. The planar interpolation methodology used a Python script that interfaced with the Paraview visualization product (Ayachit 2015).

3.1. *Results*

Figure 2 outlines the full set of integrated QoIs for the Hex8 channel (both with and without SGS model contributions). The results are as expected in that mean profiles for more dissipative schemes are over-predicted; streamwise rms is also uniformly over-predicted for the base mesh, while spanwise and vertical rms are slightly under-predicted, (see Gullbrand & Chow 2003 for a description of how accuracy influences predicted profiles). Both schemes, however, demonstrate a level of mesh convergence for the uniformly refined mesh (R1). The effect of the SGS model is small for this lower-Reynolds-number channel flow, but not negligible. In general, the element-based scheme is approximately twice as slow as the edge-based scheme at the same mesh resolution. This timing disparity is largely attributed to the larger element-node-element implicit stencil connectivity,

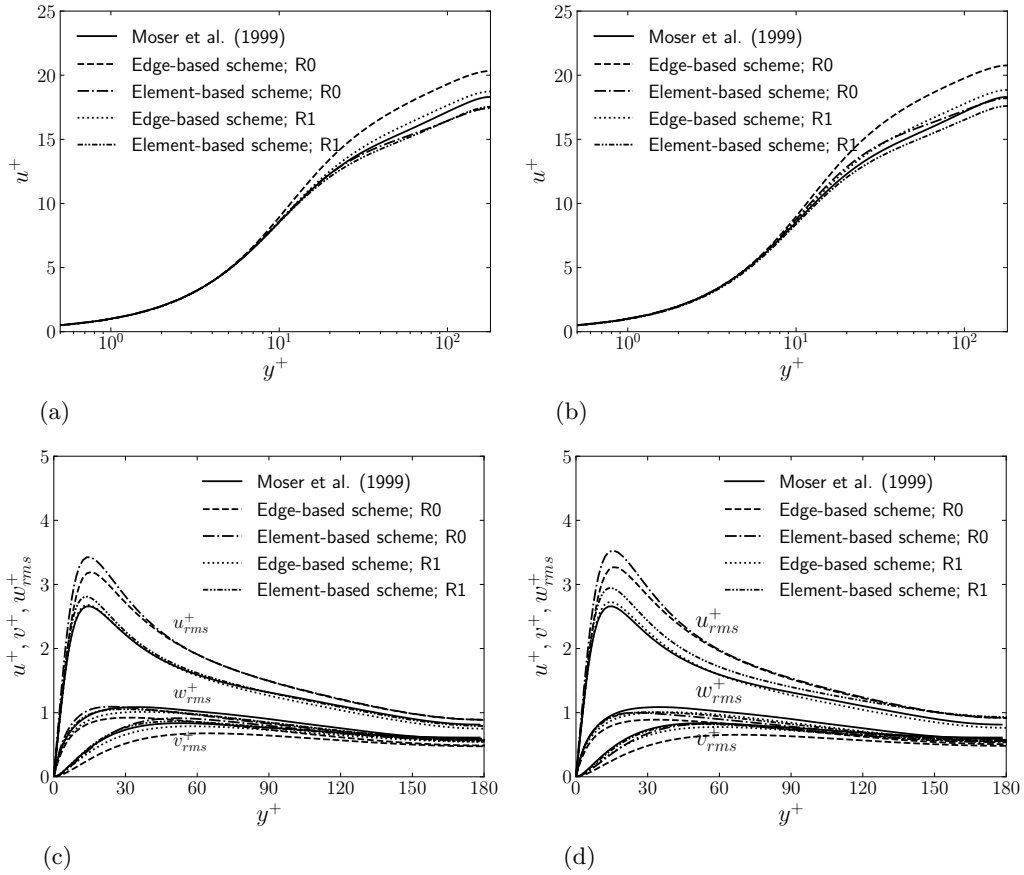

FIGURE 2. Structured Hex8 channel profile results (with and without the SGS model contributions) on both the R0 and R1 meshes: (a) without SGS, streamwise velocity; (b) WALE SGS, streamwise velocity; (c) without SGS, rms velocity fluctuations; (d) WALE SGS, rms velocity fluctuations.

which increases both matrix assembly and linear solve time, and the increased cost associated with the element-based diffusion operator.

Figure 3 outlines the integrated streamwise velocity profiles for the hybrid channel simulation. For this mesh configuration, profiles and integrated quantities are provided from the top (Tri3/Wedge6) and bottom (Quad4/Hex8) perspectives. The plots indicate that both the element- and edge-based approaches retain symmetry for this low-order statistic very well. The edge-based scheme, again, over-predicts the mean profile in a manner consistent with Hex8 results. Again, the effect of the inclusion of the LES modeling approach is small.

Figures 4 and 5 show rms velocity profiles for the simulations with and without the SGS model contributions. In both figures, non-symmetric rms velocity profiles are noted; however, they improve with mesh refinement. The transition between the Wedge6 and Tet4 element blocks is evident in the profiles (see $y^+ = 90$). This region corresponds to the location in which the highest dual-volume ratios between successive mesh-node locations are found. This transition artifact is noted for both the WALE and non-SGS

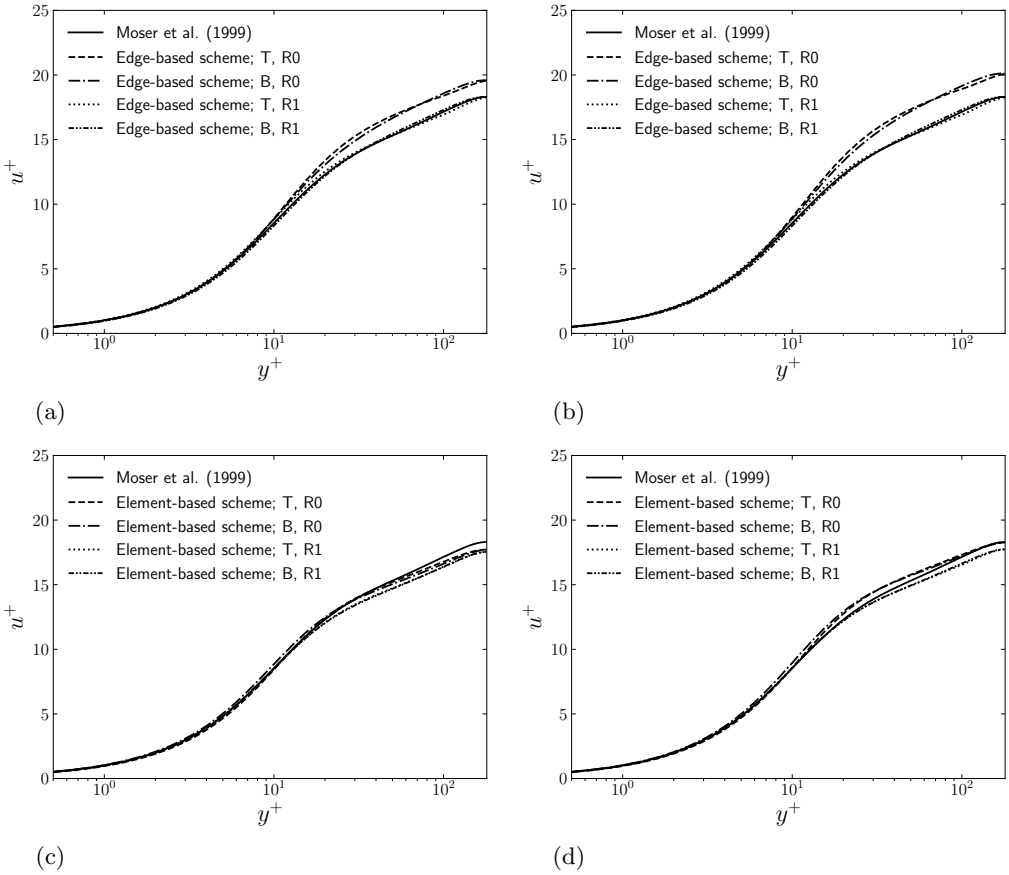

FIGURE 3. Hybrid streamwise velocity profile channel results (with and without SGS model contributions) for the edge- and element-based schemes on both the R0 and R1 meshes: (a) without SGS, edge-based; (b) WALE SGS, edge-based; (c) without SGS, element-based; (d) WALE SGS, element-based.

approaches for both numerical schemes. Therefore, core numerical dual-volume transition nuances are higher than, e.g., commutation errors. Given the use of the fully unstructured tetrahedral-based topology and near-wall Wedge6, the results are extremely encouraging.

For integrated quantities that include mean bulk velocity and skin friction, the reader is referred to Tables 1 and 2. Results indicate good symmetry for the element-based scheme versus the edge-based scheme. In fact, integrated quantities are very similar between the two mesh types.

Finally, Figure 6 illustrates an instantaneous wall shear stress at the top and bottom walls for the edge- and element-based schemes (shown for the base R0 resolution). The plot demonstrates an increased oscillation effect near the Tri3 surface, especially for the edge-based scheme. The increased spurious oscillations in the velocity field have the effect of artificially increasing the near-wall streamwise rms.

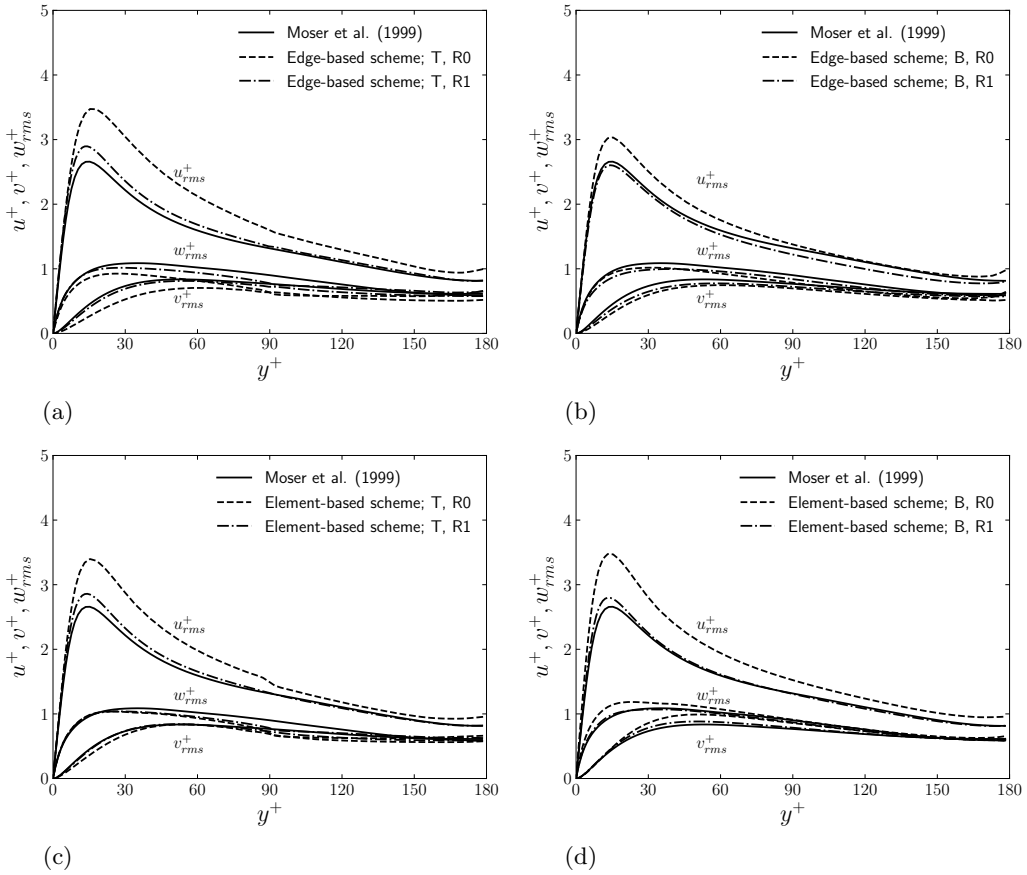

FIGURE 4. Hybrid rms profile channel results (without SGS model contributions) for the edge- and element-based scheme on both the R0 and R1 meshes: (a) edge-based, top; (b) edge-based, bottom; (c) element-based, top; (d) element-based, bottom.

	Hex8		Hybrid	
Simulation	Non-SGS	WALE	Non-SGS (T/B)	WALE (T/B)
Edge; R0	18.156	18.574	16.845/16.966	17.302/17.454
Element; R0	15.669	16.413	15.355/15.375	15.848/15.931
Edge; R1	16.403	16.523	15.586/15.814	15.574/15.815
Element; R1	15.380	15.430	15.029/15.113	15.194/15.331

TABLE 1. Bulk velocity prediction for the Hex8 and hybrid edge- and element-based schemes; theoretical value is 15.633.

	Hex8		Hybrid	
Simulation	Non-SGS	WALE	Non-SGS (T/B)	WALE (T/B)
Edge; R0	0.00607	0.00579	0.00710/0.00708	0.00677/0.00662
Element; R0	0.00813	0.00740	0.00824/0.00896	0.00779/0.00823
Edge; R1	0.00743	0.00733	0.00867/0.00784	0.00870/0.00783
Element; R1	0.00850	0.00820	0.00894/0.00897	0.00876/0.00866

TABLE 2. Skin-friction prediction for the Hex8 and hybrid edge- and element-based schemes; theoretical value is 0.00815.

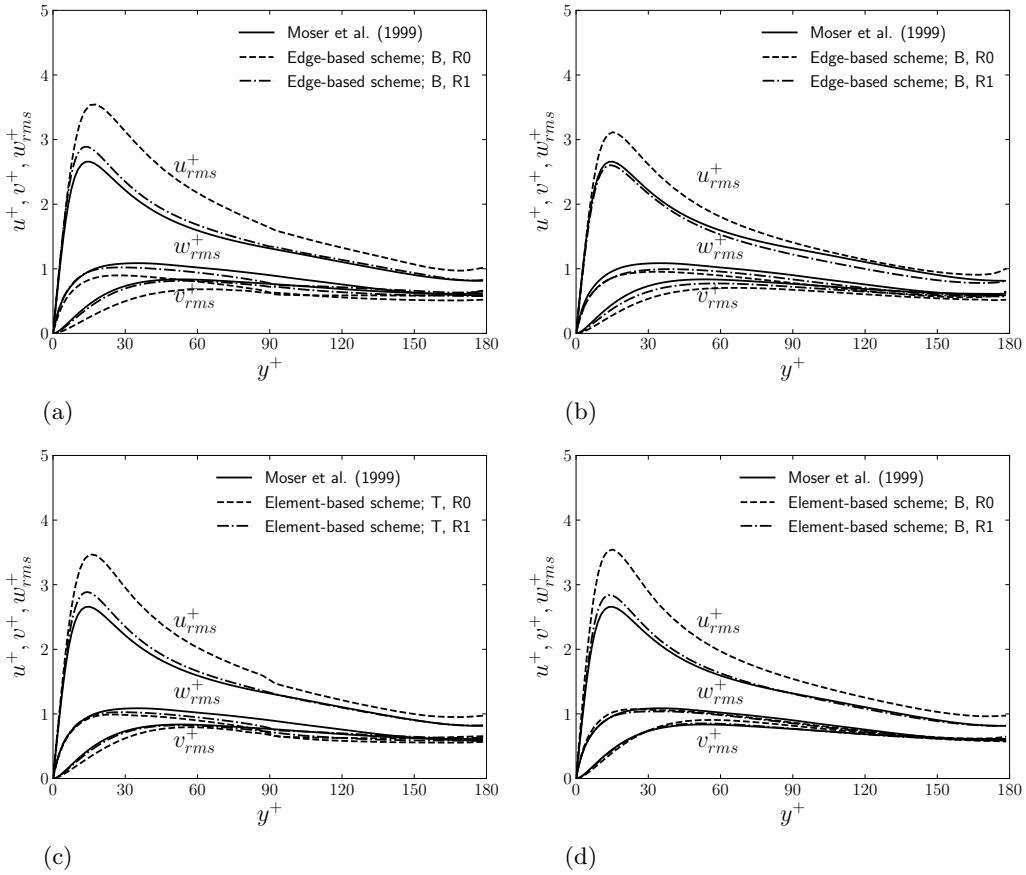

FIGURE 5. Hybrid rms profile channel results (with SGS model contributions) for the edge- and element-based schemes on both the R0 and R1 meshes: (a) edge-based, top; (b) edge-based, bottom; (c) element-based, top; (d) element-based, bottom.

4. Conclusions

In this paper, a low-Mach, low-dissipation generalized unstructured set of schemes is applied to an LES plane channel validation study. Results indicate that mean quantities are predicted reasonably well on the hybrid mesh with very acceptable symmetry observed from either the generalized unstructured or structured hexahedral mesh perspective. Although the base mesh demonstrates stronger asymmetric behavior for higher-order statistics, with mesh refinement, symmetry increases. All methods predict mean quantities well, especially with mesh refinement. Finally, the simulation study presented provides evidence that the use of both the element- and edge-based schemes is warranted for both ideal structured Hex8 meshes in addition to hybrid meshes that include hexahedral, tetrahedral, wedge, and pyramid element topologies – especially when dual-volume ratios are below a factor of two near the topological transitions.

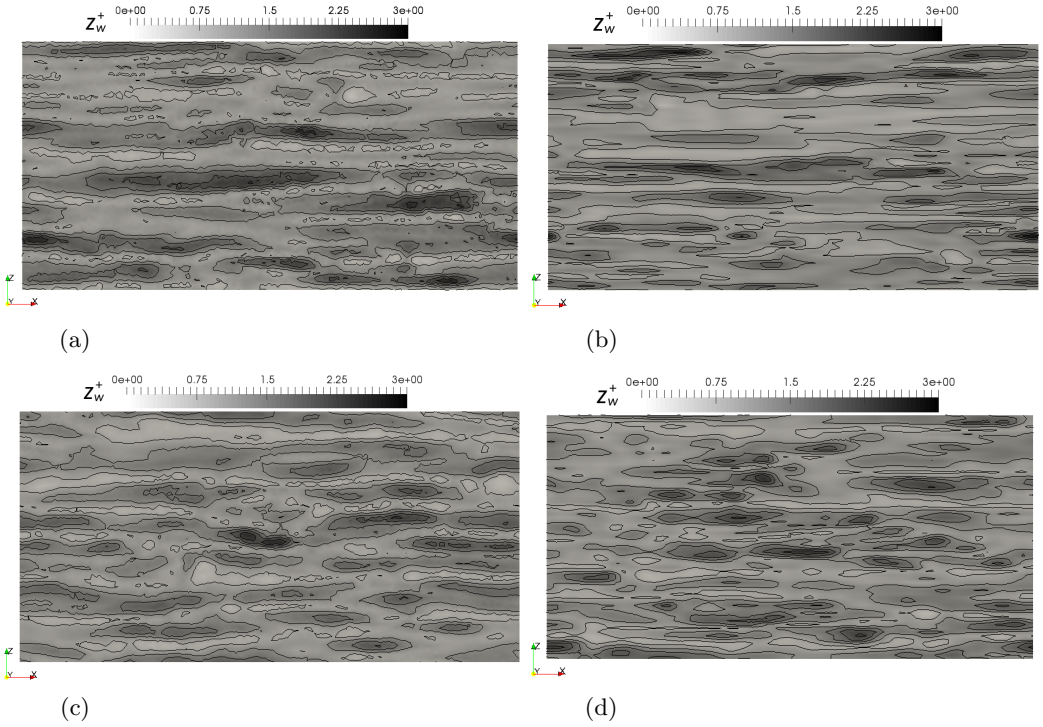

FIGURE 6. Wall shear stress profiles for the top (Tri3) and bottom (Quad4) wall boundaries using the WALE LES model (R0 base mesh refinement): (a) edge-based, top; (b) edge-based, bottom; (c) element-based, top; (d) element-based, bottom.

Acknowledgments

Sandia National Laboratories is a multi-mission laboratory managed and operated by National Technology and Engineering Solutions of Sandia, LLC., a wholly owned subsidiary of Honeywell International, Inc., for the U.S. Department of Energy's National Nuclear Security Administration under contract DE-NA0003525. This paper describes objective technical results and analysis. Any subjective views or opinions that might be expressed in the paper do not necessarily represent the views of the U.S. Department of Energy or the United States Government (SAND2018-9350 J). The authors would like to thank the Sandia National Laboratories staff Dr. Matt Barone for hybrid meshing support.

REFERENCES

AYACHIT, U. 2015 The ParaView Guide. *Kitware*, ISBN 978-1930934306.

DE WIART, C., HILLEWAERT, M., DUPONCHEEL, M. AND WINCKELMANS, G. 2014 Assessment of a discontinuous Galerkin method for the simulation of vortical flows at high Reynolds number. *Int. J. Num. Meth. Fluids* **74**, 469–493.

DOMINO, S. 2018 Design-order, non-conformal low-Mach fluid algorithms using a hybrid CVFEM/DG approach. *J. Comput. Phys.* **359**, 331–351.

DOMINO, S. P. 2006 Toward verification of formal time accuracy for a family of approx-

imate projection methods using the method of manufactured solutions. *Proceedings of the 2006 Summer Program*, Center for Turbulence Research, Stanford University, pp. 163–177.

Domino, S. P. 2014a A comparison between low-order and higher-order low-Mach discretization approaches. *Proceedings of the 2014 Summer Program*, Center for Turbulence Research, Stanford University, pp. 387–396.

Domino, S. P. 2014b Sierra low-Mach Module Nalu: theory manual. *Sandia National Laboratories SAND Series*, SAND2015-3107W.

Gullbrand, J. and Chow, F. K. 2003 The effect of numerical errors and turbulence models in large-eddy simulations of channel flow, with and without explicit filtering. *J. Fluid. Mech.* **495**, 323–341.

Ham, F., Mattson, K. and Iaccarino, G. 2006 Accurate and stable finite volume operators for unstructured flow solvers. *Annual Research Briefs*, Center for Turbulence Research, Stanford University, pp. 243–261.

Hanlin, A., Domino, S. P., Figueroa, V. and Romero, V. 2009 Validation and uncertainty quantification of Fuego simulations of calorimeter heating in a wind-driven hydrocarbon pool fire. *Sandia National Laboratories SAND Series*, SAND2009-7605.

Jansen, K. 1996 Large-eddy simulation of flow around a NACA 4412 airfoil using unstructured grids. *Annual Research Briefs*, Center for Turbulence Research, Stanford University, pp. 225–232.

Jasak, H. 1996 *Error analysis and estimation for the finite volume method with applications to fluid flow.* Ph.D. Thesis, Imperial College.

Mahesh, K., Constantinescu, G., and Moin, P. 2004 A numerical method for large-eddy simulation in complex geometries. *J. Comput. Phys.* **197**, 215–240.

Moser, R., Kim, J., and Mansour, N. 1999 Direct numerical simulation of turbulent channel flow up to $Re_\tau = 590$. *Phys. Fluids* **11**, 323–945.

Nicoud, F. and Ducros, F. 1999 Subgrid-scale stress modelling based on the square of the velocity gradient tensor. *Flow Turbul. Combust.* **62**, 183-200.

Pope, S. 2000 *Turbulent Flows.* Cambridge University Press.